

UNDERSTANDING THE POLAR ATMOSPHERIC DYNAMICS OF JUPITER AND SATURN

Justin Garland, Hampton University
Kunio Sayanagi, Hampton University

Abstract

Our project examines the mechanisms that form and maintain the cloud bands on Jupiter and Saturn by quantifying the differences between the two planets. Specifically, the spatial scales of cloud patterns as a function of latitude, which should reflect the scale of atmospheric turbulence on each of the planets, can be measured with a variety of methods. We examine this quantity using the Fast Fourier Transform (FFT) of the autocorrelation field, the Lomb-Scargle periodogram, and manual/automated feature identification. For Jupiter, we analyze data captured by JunoCam aboard the Juno spacecraft; for Saturn, we use the images from the Cassini Imaging Science Subsystem (ISS). Measurements of Jupiter's polar atmospheric turbulence are possible for the first time, enabled by images with unprecedented spatial resolution captured by JunoCam. We test the prediction that small vortices become more prevalent toward the poles and prevent cloud bands from forming at those latitudes on Jupiter, while Saturn's vortex scales do not become small enough to disrupt its banded structure. Objectives of our research include quantifying the differences between the two planets in order to test predictions of transition to polar turbulence on Jupiter and non-transition on Saturn and informing gas giant atmospheric dynamics models.

Introduction

While the visible appearance of Jupiter and Saturn are both dominated by cloud bands, their morphologies critically diverge toward the poles. Saturn's banded morphology continues up to the poles, culminating with well-organized polar vortices. In contrast, Jupiter's cloud bands only extend to around 65° latitudes with the poles exhibiting a largely chaotic arrangement of vortices. Jupiter's cloud morphology becomes turbulent toward the poles and neither pole harbors an organized polar vortex. This disparity is hypothesized to be caused by differences in the relationship between the scale of atmospheric turbulence and the planetary radius^{9,10,18,19}. In particular, these hypotheses predict that small vortices become more prevalent toward the poles. Cloud patterns on Jupiter and Saturn should exhibit the predicted latitude-dependent scales of turbulence. Previously, for Jupiter, the spatial power spectrum of the cloud reflectivity maps has been computed to analyze the scale of clouds between $\pm 60^\circ$ latitudes⁵. Jupiter's poles were never imaged in visible light before Juno's arrival, and thus the polar latitudes were not included in previous analyses. Jupiter's polar cloud spatial scales thus remain unexamined, a primary goal of this work. Saturn's polar cloud morphology has been documented using high resolution images captured during Cassini's high inclination Grand Finale orbits²⁰; however, its spatial scales also remain to be measured.

We will first discuss each of our three methods (FFT, Lomb-Scargle, and manual/automated identification). Then, we

will detail the JunoCam and Cassini datasets these methods are applied to. Finally, our initial results and next steps are detailed.

Methods

FFT Autocorrelation

Our first method involves a two-dimensional Fast Fourier Transform (FFT) of the autocorrelation field. An autocorrelation field is generated by computing the correlation of an image containing cloud features with a copy of itself as it is shifted horizontally by a “lag” amount of pixels. The correlation value without any shift would be 1.0, indicating no difference in the correlated images, and the correlation decreases in most images as the horizontal shift grows. The fall-off distance in the autocorrelation field can characterize the spatial scales contained in the image. Pixel lags corresponding to dominate scales of features will have higher correlation values in the resulting plot. This process in the form of an equation is summarized as:

$$(1) \quad C_{aa}(k) = \sum_{n=-N/2}^{N/2} a(n+k) \bar{a}(n)$$

where $C_{aa}(k)$ is the autocorrelation field at a lag k , N is the width of the input image in pixels, and \bar{a} is a copy of the original image $a(n+k)$ that is unshifted. Taking the square of the FFT of the resultant autocorrelation field gives a power spectrum, which peaks at lags that contain the dominant scales of features in the image. By computing the power spectrum for small portions of Jupiter and Saturn’s surfaces, we can measure the change in the spectral characteristics in latitude. The advantage of the FFT method is that it is sensitive to east-west, north-south anisotropy, which is predicted to be important in determining jet- vs. vortex-dominated flow regimes on Jupiter²⁶.

Lomb-Scargle Periodogram

The Lomb-Scargle (LS) periodogram method¹⁰ has previously been applied for images of Jupiter⁶. The LS method performs a spectral transform similar to the FFT, except that the source data sampling can be incomplete and irregular, which is an advantage in our project as JunoCam data rarely provides full longitudinal data at any single latitude. It also allows comparison of spectra with different intensity levels allowing better comparisons between instruments. Using the LS method, we measure the scale of clouds in the east-west directions as a function of latitude in a similar manner to the previous method, allowing these two calculations to support the others’ result. We have only initially examined a treatment of JunoCam and Cassini data using the LS method.

Feature Identification: Manual

We extend previous work^{15,23} on manually identifying cloud features and their spatial scales by searching for features in JunoCam and Cassini images. By plotting these features to examine their occurrence and size by latitude, we provide another check of the previous two methods. This is done by simply visually inspecting each JunoCam and Cassini image and circling and sorting various cloud features by size and type. This provides a measure, though biased by human judgement, of feature scale in each image that may be compared to the results of the FFT and LS methods.

Feature Identification: Automated

Manual identification can itself be automated via machine learning techniques. Convolutional neural networks (CNNs) are a class of deep-learning neural networks commonly used to identify features in images.

They consist of an input layer of data which is passed through several “convolutional” layers. These perform cross-correlation operations on the data based on automatically generated filters learnable from training datasets. These filters do not require human guided definitions, allowing CNNs to better resolve features in the raw data without loss of information. They output maps of extent and number of identified features found in the image. Many open source CNN codes exist, and the technique has been successfully used in planetary science. Other flavors of neural network have been used to identify impact craters in images^{1,21,23} and in 2016 Cohen et al. showed preliminary results of a CNN outperforming previous methods used on the same dataset⁴. CNNs have also been used to identify volcanic rootless cones and transverse aeolian ridges in Mars Reconnaissance Orbiter datasets¹¹. More relevant to atmospheric science, Pankratius et al. utilized a CNN to identify gravity waves on Earth from lee cloud wave patterns in Moderate Resolution Imaging Spectroradiometer data, achieving a 96 percent identification rate¹². We are working to develop an open-source pipeline utilizing the PyTorch¹⁶ framework to automatically identify cloud features using a CNN with my manual identifications as training sets. PyTorch was selected due to its flexibility and computational speed in initial experimentation. This code will allow new JunoCam flybys to be analyzed promptly after release and may be extended to the full library of Cassini ISS data.

Datasets

JunoCam

JunoCam is a 58 degree field of view camera aboard the Juno spacecraft with 4 filters: red (600-800 nm), green (500-600 nm), blue (420-520 nm), and a methane band (880-900 nm). Filters were chosen to meet

signal to noise requirements imaging the poles and to allow reconstruction of true-color images as a public outreach tool⁶. Juno’s close passes to Jupiter give the camera a resolution of 3 kilometers per pixel around the equator during “perijove” and a resolution of 50 km per pixel over the poles⁶. This represents an order of magnitude improvement over Cassini images of Jupiter^{6,14}. RGB and methane images are taken as strips during successive 30 second rotations of the spacecraft. JunoCam images become publicly available on the Planetary Data System (PDS)⁷ a few months after they are downlinked to Earth. We process images using the Integrated Software for Imagers and Spectrometers (ISIS3) software developed by the U.S. Geological Survey²⁴, which can calibrate and map-project images of planetary bodies captured by various missions. ISIS3 Cassini ISS modules have been actively used at Hampton University for various analyses of Saturn². The JunoCam module was publicly released earlier this year, which we have successfully used to process all presently released JunoCam images. My pipeline accounts for some of the difficulties presented by JunoCam’s design. Each image consists of framelets, taken during each spacecraft rotation, which must be first mapped to preserve pointing data then mosaiced together into a final image. The result of this mapping and mosaicing procedure is shown in Figure 1.

Cassini

We focus on Cassini ISS views in the CB2 (750 nm), MT2 (727 nm), and MT3 (889 nm) narrow-band filters of Saturn to compare the morphology of clouds between the two planets¹⁵. Additionally, we have mapped images from Cassini’s encounter with Jupiter in the same filters to serve as a check on results from JunoCam at lower latitudes. These filters overlap some of JunoCam’s, allowing comparisons at the same atmospheric levels

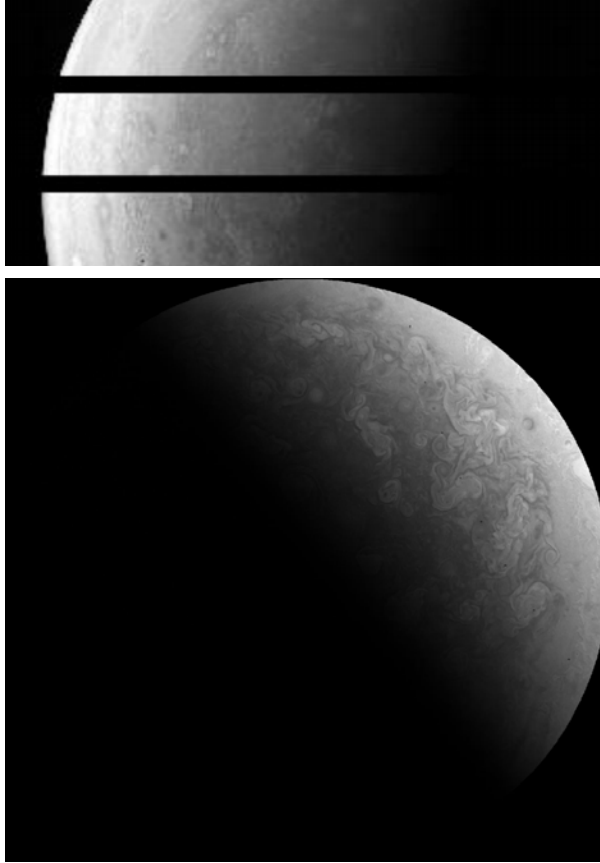


Figure 1: Examples of raw (upper) and final (lower) JunoCam images from data processed with ISIS3. The raw image shows three framelet strips which must be separately map projected before mosaicing into a final image. This image is a polar-projected, red-filter view from perijove 4 data.

between the two datasets. They are also frequently used and provide a large dataset both for analysis and training CNNs. Images have been selected that both have sufficient spatial resolution to be analyzed and that cover a large range of latitudes, focused on the poles. The project utilizes publicly available data on the PDS. Interestingly for Jupiter, by analyzing the same regions of the planet in the different spatial resolutions provided by Cassini and JunoCam we may be able to probe the scales at which turbulent flow is dissipated on the planet. This adds further value to examining Cassini data of Jupiter.

Initial Results

We have completed two main tasks in our first year of work: mapping and mosaicing JunoCam images and computing the power spectrum of individual images. We have developed a code to compute the FFT of the autocorrelation field for JunoCam images. An initial autocorrelation field may be seen in Figures 2, and 3. From our rough power spectra, it is clear that additional corrections to the public outreach JunoCam data are necessary. Namely, brightness variations in the images need to be corrected and the navigation of the images must be improved before a dataset-wide search for feature scales can be commenced using either our already implemented FFT and LS methods.

We have also begun manual identification of features in the JunoCam dataset. With the assistance of recent undergraduate members of our research group, this task should be completed for currently available JunoCam data in the coming months.

Finally, we have begun testing a CNN treatment of this manual identification set using a PyTorch-based pipeline. This, too, relies on correct spacecraft navigation to correctly identify scales of cloud features by latitude. This issue of navigation and data handling is the current focus of our efforts.

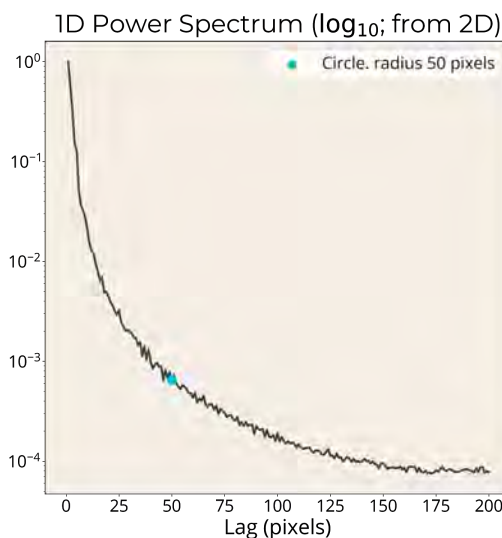
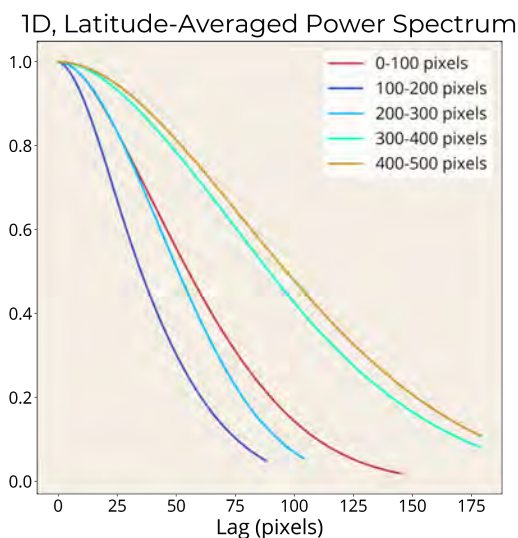
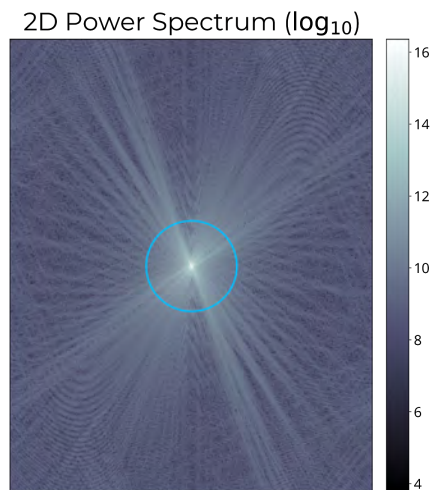
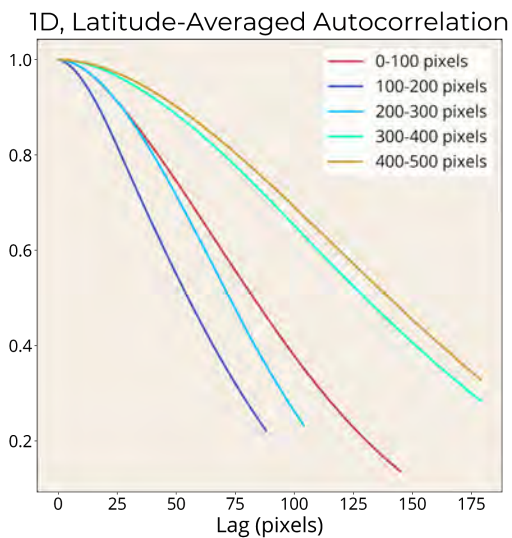


Figure 2: One-dimensional autocorrelation field (upper) and power spectrum (lower) from a mid-latitude JunoCam image. Each line represents an averaged 100 pixel latitude band, showing how the fall-off of the autocorrelation varies with latitude. The power spectrum is the normalized, squared FFT of the upper plot. This retrieval is primarily sensitive to brightness variations in the image and projected shape rather than the characteristic feature scale of clouds.

Figure 3: Two-dimensional power spectrum (upper) and its one-dimensional expression (lower) from a mid-latitude JunoCam image. The 1D power spectrum is found by summing rings about the center of the 2D spectrum; the blue ring in the upper plot corresponds to the blue point in the lower plot.

Future Work

The spacecraft pointing data available on the PDS used by ISIS3 to determine what

latitude each pixel in an image falls at is often far from accurate, by up to 30 degrees latitude in some extreme cases. We have begun experimentation using the OMINAS software to correct these errors via limb-fitting and comparisons to known features visible in the images²⁶. OMINAS, like ISIS3, implements

both a JunoCam and Cassini camera model. This has led to a relatively straightforward process of applying the limb-fitting and named feature methods of correcting spacecraft pointing to our data. We will use OMINAS to update the SPICE (Spacraft, Planet, Instrument, “C-matrix”, Events) kernel attached to each mapped image with corrected latitude and longitude information. This corrected kernel may then be sent back to our existing ISIS3 pipeline. This processing step is the immediate step we will take towards our proposed measurements.

Our other measurements (FFT, LS, automated identification) heavily depend on this correction; however, these measurement methods are all operational to various extents. The most complete work is with our FFT and LS pipelines, which will be applied to the full JunoCam and Cassini datasets once OMINAS is applied to the data. We will then focus our efforts on completing our PyTorch CNN code. By comparing these complimentary results, we will have a robust view of the primary feature scales on Jupiter and Saturn as a function of latitude. Comparing results for the two planets will achieve our goal of quantifying the transition of banded structures to turbulence at Jupiter’s poles and Saturn’s lack of such a transition.

Acknowledgements

The author would like to thank Dr. Kunio Sayanagi and John Blalock for their advisement and support. Additionally, the Virginia Space Grant Consortium’s financial support of this project is much appreciated. We would also like to thank the USGS for their work on ISIS3 as well as Joseph Spitale and other contributors to the OMINAS software.

References

1. Bandeira, L., Ding, W., Stepinski, T.F., 2012. *Adv. Space Res.* 49, 64–74.
2. Blalock, J. J., Sayanagi, K. M., Ingersoll, A. P., et al., 2017. *American Astronomical Society, DPS* 49, 205.11
3. Brueshaber, S. R., Sayanagi, K.M., 2016. *American Astronomical Society, DPS* 48, 501.01
4. Cohen, J. P., Lo, H. Z., Lu, T., Ding, W., 2016. *Proceedings of the 47th Lunar and Planetary Science Conference, Abstract # 1143.*
5. Harrington, J., Dowling, T. E., Baron, R. L., 1996b. *Icarus* 124, p. 32-44
6. Hansen, C. J., Caplinger, M. A., Ingersoll, A., et al., 2014. *Space Sci. Rev.*
7. JunoCam Online Data Volumes (PDS): <https://pds-imaging.jpl.nasa.gov/volumes/juno.html>
8. Lomb, N. R., 1976. *Astrophysics and Space Science*, 39:447–462.
9. O’Neill, M. E, Emanuel, K. A., Flierl, G. R., 2015. *Nature Geosci.* 8, p. 523-526
10. O’Neill, M. E, Emanuel, K. A., Flierl, G. R., 2016. *J. Atmos. Sci.* 73, p. 1841-1855
11. Palafox, L. F., Hamilton, C. W., Scheidt, S. P., Alvarez, A. M., 2017. *Computers & Geosciences* 101, p. 48-56.
12. Pankratius, V., Li, J. D., Rude, C. M., Gowanlock, M., Herring, T., 2017. *American Geophysical Union, 2017 Fall Meeting, IN11E-01.*
13. Penny, A. B., Showman, A. P., Choi, D. S., 2010. *J. Geophys. Res.* 115, E02001
14. Porco, C. C., West, R. A., McEwen, A., Del Genio, A. D., Ingersoll, A. P., Thomas, P., Squyres, S., Dones, L., Murray, C. D., Johnson, T. V., Burns, J. A., Brahic, A., Neukum, G., Veverka, J., Barbara, J. M., Denk, T., Evans, M., Ferrier, J. J., Geissler, P., Helfenstein,

- T., Roatsch, T., Throop, H., Tiscareno, M., Vasavada, A.R., 2003. *Science* 299, 1541-1547.
15. Porco, C. C., West, R. A., Squyres, S., McEwen, A., Thomas, P., Murray, C. D., Del Genio, A., Ingersoll, A. P., Johnson, T. V., Neukum, G., Veverka, J., Dones, L., Brahic, A., Burns, J. A., Haemmerle, V., 2004. *Space Science Reviews* 115, 363-497.
 16. PyTorch: <https://pytorch.org/>
 17. Richard A. McCray, Bernard F. Burke, et al., 2001. *Vision and Voyages for Planetary Science in the Decade 2013-2022*. The National Academies Press.
 18. Sayanagi, K. M., Showman, A. P., Dowling, T. E., 2008. *J. Atmos. Sci.* 65, p. 3947
 19. Sayanagi, K. M., et al., 2016. Chapter 12 of “Saturn in the 21st Century” In Press at Cambridge U. Press.
 20. Sayanagi, K. M., Blalock, J. J., Dyudina, U. A., Ewald, S. P., Ingersoll, A., P., 2017. *Icarus* 285, p. 68-82
 21. Stepinski, T. F., Ding, W., Vilalta, R., 2012. Detecting impact craters in planetary images using machine learning 1, pp. 146–159.
 22. Trammell, H. J., Li, L., Jiang, X., Pan, Y., Smith, M. A., et al., 2016. *J. Geophys. Res.* 121, p. 1814-1826
 23. Urbach, E. R., Stepinski, T.F., 2009. *Planet. Space Sci.* 57, 880–887
 24. USGS Integrated Software for Imagers and Spectrometers (ISIS3): <https://isis.astrogeology.usgs.gov/index.html>
 25. Vasavada, A. R., Showman, A. P., 2005. *Rep. Prog. Phys.* 68, p. 1935-1996
 26. OMINAS software documentation: <https://nasa.github.io/ominas/guides/useguide.html>